Chapter 9
Wrinkling on Covalently Anchored Hydrogels

Chya-Yan Liaw, Jorge Pereyra, and Murat Guvendiren

9.1 Introduction

Surface patterns are commonly observed in nature and the human body, such as mucosal folds on the intestinal wall which facilitate rapid exchange of mass, nutrient, and waste [1]; wrinkles on the human skin [2]; folds in the human brain to increase surface area [3], and buckling protrusions on tumor surfaces which are believed to promote tumor invasion [4–5]. While patterns in nature provide important functions, surface instabilities on hydrogels have generally been considered as undesirable defects that need to be avoided. Until recently, increasing theoretical and experimental studies have been reported to predict and control the formation of surface patterns enabling the use of surface instabilities for a wide range of applications including sensors, optical devices, micro-/nano-fabrication tools, and bioengineering [6].

Hydrogels are three-dimensional networks of polymers that are capable of absorbing and retaining large amounts of water. The physical and chemical properties of hydrogels closely mimic natural living tissues; therefore, the formation of surface patterns on hydrogels has numerous potential applications in tissue engineering, biosensing, and drug delivery applications.

The use of surface patterns in soft hydrogels was reported as far back as the mid-nineteenth century in the fine art reproduction process known as "collotype printing" [7]. In the process, the printing plate was coated with a light-sensitive dichromated gelatin film and exposed to light under a photographic negative. Gelatin hardened selectively, producing surface patterns and wrinkles, upon swelling. Wrinkles varied in their ink/water absorption capacity, which gives rise to a delicate continuous-tone effect [8]. A similar phenomenon was later reported by

C.-Y. Liaw · J. Pereyra · M. Guvendiren (✉)
Otto H. York Department of Chemical and Materials Engineering,
New Jersey Institute of Technology, Newark, NJ, USA
e-mail: muratg@njit.edu

C. M. González-Henríquez, J. Rodríguez-Hernández (eds.), *Wrinkled Polymer Surfaces*, https://doi.org/10.1007/978-3-030-05123-5_9

Tanaka et al. by swelling polyacrylamide hydrogels in water [9]. Following these observations, many experimental and theoretical studies have been carried out to further exploit the surface instabilities in hydrogels.

In this chapter, we focus on the formation of surface instabilities in confined hydrogels. We first classify the types and mechanisms of the instability patterns. A detailed review on commonly used hydrogel systems to generate surface instabilities is given. Finally, a brief overview of the applications and challenges associated with the use of hydrogel instability patterns is given.

9.2 Types and Mechanisms of Hydrogel Surface Instabilities

Surface patterns in hydrogels are usually induced by lateral confinement of the hydrogel while undergoing large volume changes mainly due to swelling. They hydrogels can be classified into three main systems according to the generation of the confinement: (1) uniform and soft hydrogel attached on a stiff substrate [10–13], (2) stiff hydrogel layer on top of a compliant foundation [14], and (3) hydrogel with depth-wise cross-linking gradients [15–18] (Fig. 9.1). In the first system, a homogeneously cross-linked hydrogel is bonded to a stiff substrate. This system also includes polyelectrolyte multilayers (PEM) prepared by layer-by-layer (LBL) deposition. In the second system, a bilayer configuration consists of a rigid hydrogel layer on top of a compliant support. The support layer can be the same hydrogel or a different polymer/hydrogel. In the third system, a hydrogel film with a depth-wise gradient in cross-linking (or mechanical properties) is prepared on a substrate. The modulus gradient can be generated due to oxygen inhibition during UV curing process [18] or the infusion of reactive chemicals [15] into the hydrogel.

The possible mechanisms of pattern formation are depicted in Figs. 9.2 and 9.3. The general principle of the formation of surface instability involves lateral confinement in combination with an in-plane compressive strain ε_M (or mismatch strain) in the hydrogel film. The compressive strain ε_M can be caused by either volume expansion of the surface layer (Fig. 9.2a, path A) or shrinkage of the bottom layer (Fig. 9.2b, path B). When the compressive strain exceeds a critical value, the surface becomes unstable and spontaneously forms surface waves. In path A, the top layer

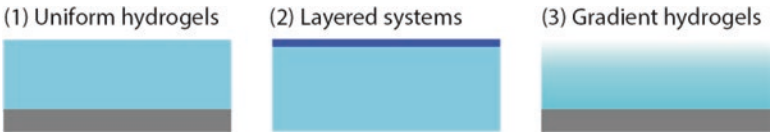

Fig. 9.1 Three types of film structure systems widely used in generating surface instability patterns: (*1*) uniform hydrogels with homogeneous cross-linking fixed on a rigid substrate, (*2*) layered film structures consist of a stiff hydrogel on a compliant hydrogel, (*3*) hydrogels with a gradual change of physical properties (e.g., modulus or polymer concentrations) and/or chemical compositions along the film thickness

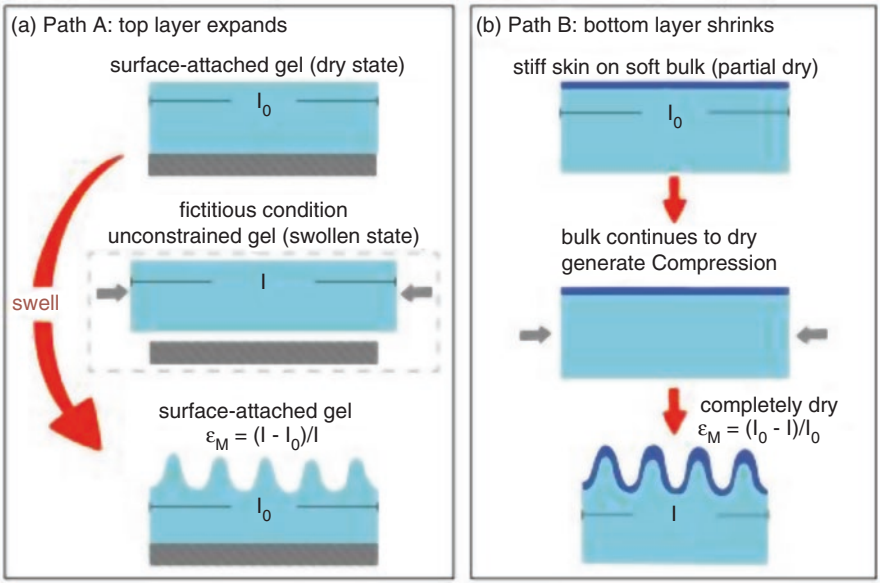

Fig. 9.2 Schematic diagram showing the mechanism of the development of surface instability patterns in hydrogels due to mistached strain. The mismatched strain can arise from (**a**) volume expansion of the top layer or (**b**) shrinkage of the bottom layer. Note that the image in the dashed box shows a fictitious step which helps to better understand. The real deformation steps are guided by the red arrows

with an initial length l_0 is able to swell more than the bottom layer when subjected to an external stimulus, such as solvent diffusion or temperature change creating an anisotropic swelling. Let us first consider swelling of an unconstrained gel (shown in the dashed box). It can swell isotropically and reach its stress-free state with a final length of l. However, in the real situation, the gel is anchored on the substrate, which prohibits it from fully expanding to an equilibrium state. Therefore, the top layer is experiencing an equibiaxial compressive strain, which is equal to $(l-l_0)/l$. Note that the first two systems shown in Fig. 9.1 form surface instabilities normally through path A. For system 1, a uniform soft gel layer (as shown in blue in Fig. 9.2a) is bonded to a stiff substrate (as shown in gray), such as glass slides or silicon wafers. In the case of system 2, a stiff, swelling layer (blue) is placed on top of a soft non-swelling thick foundation (gray). The two layers in system 2 are usually composed of the same hydrogel but with different swelling and mechanical properties. In contrast, there are only a few reports showing surface instability of hydrogels induced through path B, and most of the observations are during drying/shrinking of hydrogels.

When compared to surface patterns produced in uniform hydrogel films, the wrinkles prepared in depth-wise gradient films (system 3) are much smoother. The gradients in physical and mechanical properties across the thickness of the hydrogels have been reported in two opposite directions. In the first case (Fig. 9.3a),

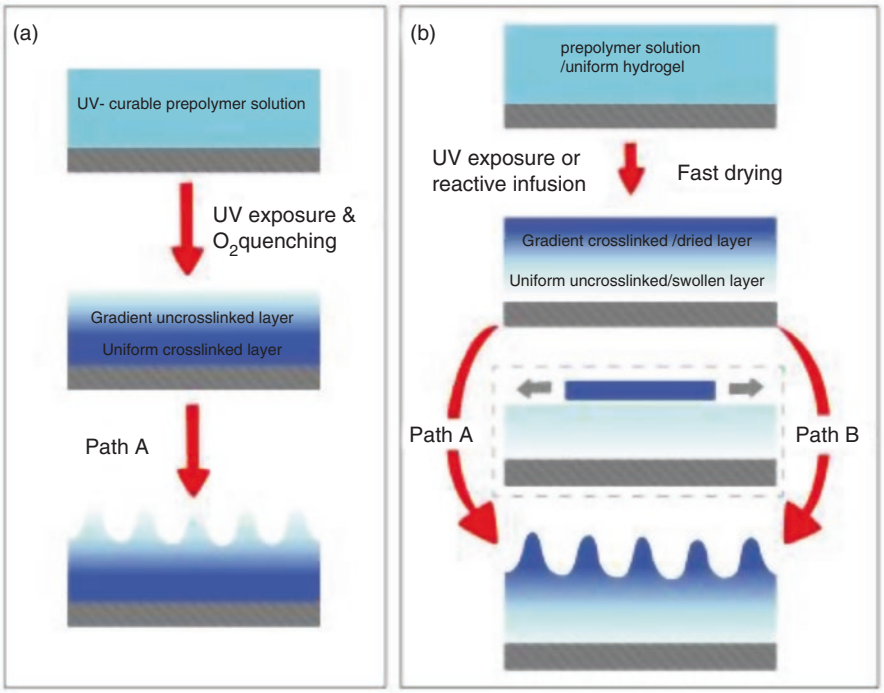

Fig. 9.3 Schematic illustrations showing the strategies to develop depth-wise gradient in hydrogels. (**a**) An uncross-linked gradient top layer and a uniform cross-linked bottom layer. (**b**) A cross-linked or drier gradient top layer and a uniform uncross-linked or swollen bottom layer. The image shown in the dashed box indicates an intermediate state of the film at which the film is under tension

a modulus gradient with a soft top layer that gradually stiffened with depth was developed. Normally, the hydrogel films are prepared by depositing a UV-curable prepolymer solution and exposing the film to UV in the presence of oxygen. Due to the quenching of free radicals by oxygen, which inhibits cross-linking toward the top layer, a modulus gradient was developed. Subsequent immersion of the film in a "good solvent," i.e., polymer is soluble in this solvent, induces anisotropic swelling of the film and, thus, produces biaxial compressive stress within the film, as described in path A. In the second case (Fig. 9.3b), a stiff skin layer forms at the surface above a soft foundation at the early stage of curing (path A) or drying (path B). In the case of the cure-induced gradient, the cured stiff skin layer is created by infusing reactive cross-linkers into the hydrogel film or by exposing the hydrogel film to a light with low penetration depth. Alternatively, fast-drying hydrogel at low humidity also experiences partial dehydration, which leads to the formation of a glassy skin layer. It should be noted that at this stage, the outer layer is drier or with higher cross-linking density and thus contracts more than the bulk. In other words, the skin layer is subject to a tensile stress (as shown in the dashed box) [19–20]. When the hydrogel film is immersed in a solvent, the compressive stress exerted by

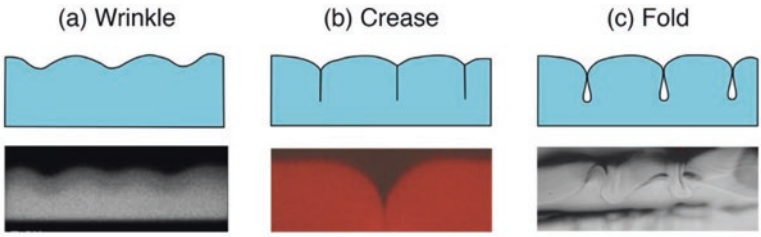

Fig. 9.4 Schematics (top row) and optical images (bottom row) showing the three most common types of surface instabilities found in constrained hydrogels. The optical images show the cross section of (**a**) polyHEMA [17], (**b**) polyNIPAM [25], (**c**) polyNIPAM [14] hydrogels

the substrate progressively increases and finally overcomes the opposing tensile stress (path A). The explanation is similar to the mechanism first proposed by Basu et al. for acrylate coatings during the UV curing process [20]. Whereas in the drying hydrogel system, the contraction of the bulk due to subsequent drying results in the generation of compressive stress in the skin layer, which also leads to the formation of surface instability (path B). This phenomenon is similar to the poly(dimethylsiloxane) system in which a mechanically stretched poly(dimethylsiloxane) (PDMS) is exposed to UV/ozone radiation, thus creating a stiff oxidized surface layer, followed by strain release [21].

Considering the three main hydrogel systems described above, various modes of surface instabilities, including wrinkling, creasing, folding, period doubling, and ridging, were reported both experimentally and theoretically (Fig. 9.4). Wrinkles represent uniform and sinusoidal deformations. Creases are nonlinear deformations forming sharp self-contacting indentations with localized large strains [22–23]. Other instability modes such as folds and ridges also represent localized strains and are typically evolved from wrinkles. When the mismatch stress between the film and substrate is low and the applied strain is far beyond the onset of wrinkles, wrinkles double their period and form folds. In contrast, when the strain mismatch is high, wrinkles evolve into ridges, which form spaced-out and large aspect ratio peaks. The patterns arising from the surface instabilities can be either irreversible or reversible. Irreversible patterns are present after they are induced and can no longer be erased, while reversible patterns show the reversible formation of patterns when materials subject to cycles of the loading-unloading processes, such as swelling/drying or heating/cooling. The reversibility of the patterns is mainly dependent on the film thickness, the cross-linking degree, and the gradient, as well as the modulus of the substrate [24].

Wang and Zhao developed a general three-dimensional phase diagram using a plane-strain finite element model to define the conditions for each type of the surface instabilities with respect to three dimensionless parameters (Fig. 9.5). This phase diagram is originally designed for uniform layered hydrogels (system 1 and 2). For this system, the dimensionless parameters are film to substrate modulus ratio (E_f/E_s), mismatch strain within the film ε_M, and normalized adhesion energy ($\Gamma/E_s t$, where Γ is the adhesion energy per unit area between the film and substrate, and t is

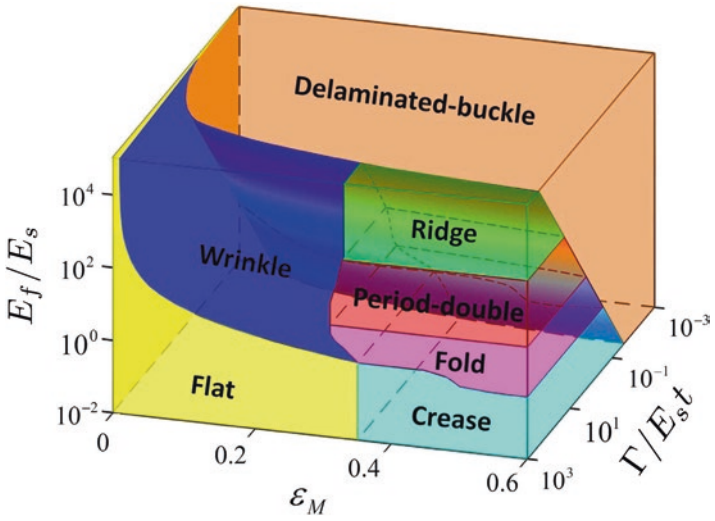

Fig. 9.5 Numerically simulated phase diagram showing various types of surface instabilities determined by three dimensionless parameters: mismatch strain ε_M, modulus ratio of the film and substrate E_f/E_s, and the normalized adhesion energy $\Gamma/E_s t$ (t is the film thickness). (Reproduced with permission from Ref. [34])

the film thickness). The moduli of hydrogels are generally measured using an atomic force microscope or a tensile tester [16, 18, 26]. The mismatch strain within the hydrogel film can be measured by determining the linear expansion of unconstrained hydrogels with identical composition as the constrained counterpart [11]. The adhesion energy between the hydrogel and the substrate can be enhanced by treating the substrate with adhesion promoters (e.g., trimethoxysilane) [11, 17–18]. For well-bonded systems, hydrogels with E_f/E_s in the range of 10^0–10^4 generally develop wrinkles when the mismatch strain is small ($\varepsilon_M = 0.05$–0.25). A great example can be found in natural mucosal tissues, where surface wrinkling and folding are crucial for the biological function. Mucosae consist of a stiff and collagenous mucosal layer and a soft, loosely connected elastin and collagen submucosal layer constrained on a much stiffer muscular layer. Volumetric growth in the mucosal layer could lead to the formation of surface wrinkling or transform into folds or period double when mismatch strains become larger ($\varepsilon_M > 0.3$) [27]. Other biological tissues [28] and engineered hydrogels [14, 29] also show similar layered structures and wrinkling/folding phenomena. Unlike wrinkles and folds, creases are generally developed in uniform hydrogel films without hard skin [5, 9, 11]. Biot's classical linear perturbation analysis failed to capture the critical condition for the onset of creases. Until recently, Hohlfeld and Mahadevan simulated the onset of creases numerically and found that a critical strain value $\varepsilon_M \approx 0.35$ [30], which does not depend on the modulus and thickness of the material. Many experimental studies showed remarkable agreement with this value [11, 31]. For instance, Trujillo et al. reported that the onset of creasing in swelling polyacrylamide-based hydrogels occurred at a critical strain equal to 0.33 [11].

It is worthwhile mentioning that it is not easy to directly measure the compressive strain ε_M in the case of surface-attached hydrogels. For example, to calculate the compressive strain in constrained hydrogels, Trujillo et al. measured the linear extent of swelling for unconstrained hydrogels. However, they mentioned that it was difficult to handle the unsupported films due to the fragility of the films. The swelling ratio α_c, defined as the ratio of the film thickness in a swollen state and in a dry state, is commonly used as an alternative method to determine the onset of surface instability. The range of the reported critical values is wide [32]. For example, Trujillo et al. reported a critical swelling ratio for the onset of creases of about 2 for the polyacrylamide hydrogel system [11], while Dervaux et al. found a low instability threshold of roughly 1.5 for their ring polyacrylamide model [5]. On the other hand, Guvendiren et al. found that α_c is about 1.12 for the onset of wrinkling of the polyHEMA system [16]. Recently, Han et al. showed that α_c of surface wrinkling observed for a model system of layer-by-layer PVP/PAA hydrogel was higher than 2 [33].

9.3 Commonly Used Hydrogel Systems for Surface Patterning

The formation of surface instability morphologies on a hydrogel surface is the result of a large change in osmotic pressure within the gel. The osmotic pressure can be varied by changing a variety of factors, such as solvent composition, temperature, pH of the solvent, ionic strength, etc. Here, we classify the external stimuli into three major types: (1) solvent, (2) temperature, and (3) others (such as electric field and light).

9.3.1 Solvent-Induced Systems

9.3.1.1 Polyacrylamide(pAAM)-Based

Polyacrylamide-based hydrogels are widely used as a model system for investigating surface instability since their mechanical and swelling properties can be easily tuned by controlling the chemical composition. The pAAM hydrogels are generally prepared by copolymerizing acrylamide monomers with anionic monomers, such as sodium acrylate (SA) in the presence of bifunctional cross-linkers (bisacrylamide), and chemically attached on a rigid substrate. The osmotic pressure and degree of swelling within the pAAM/SA gels can be varied by adjusting the amount of sodium acrylate monomers, and the film modulus is varied by changing the concentration of monomers and cross-linkers. Pioneering works by Tanaka et al. have demonstrated the kinetic evolution of surface patterns of an ionized acrylamide gel in a petri dish swelled in water. They suggested that the critical osmotic pressure for the onset of

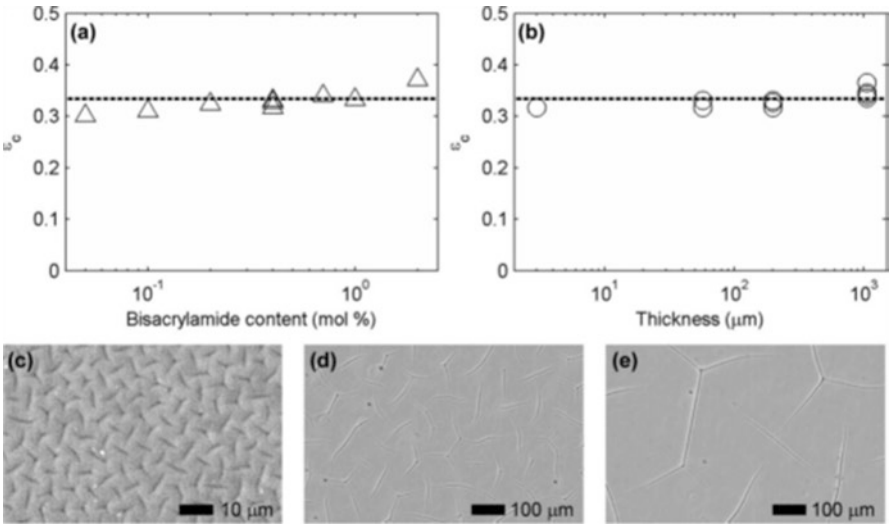

Fig. 9.6 The critical strain for the onset of creasing as a function of the (**a**) concentration of cross-linkers (at a constant thickness of 200 μm) and (**b**) gel thickness at a constant degree of cross-linking (0.4 mol % bisacrylamide). In both cases, the critical strain varies only slightly, which is in good agreement with the prediction of Biot, as shown by the dashed lines. (**c–e**) Optical images of crease structures as a function of the initial film thickness of (**c**) 3 μm, (**d**) 40 μm, (**e**) 160 μm. (Reproduced with permission from Ref. [11])

surface instability depends on Young's modulus of the gel but independent of the gel thickness [9]. Later, Trujillo et al. used polyacrylamide copolymer hydrogels as a model system to investigate the critical condition for the onset of creasing (Fig. 9.6) [11]. They found that the critical strain was $\varepsilon_M \approx 0.33$ (0.30–0.37) and the swelling ratio was $\alpha_c \approx 1.5$–2. These values only varied slightly as the film modulus changed from 0.6 to 24 kPa and were independent of the investigated gel thickness (3 μm–1 mm). The value of ε_M agrees well with the theoretical predictions proposed by Biot for rubber under equibiaxial compression using linear perturbation analysis [35]. In addition, results obtained from a prior experimental study of rubber with moduli on the order of 1 MPa swelled in n-decane showed an almost identical value of ε_M [36], indicating that this critical strain value is nearly universal for swell-induced surface instability in confined polymer layers. ε_M may increase when scaling down the film thickness as the capillary force and elasticity become comparable. A follow-up study by the same research group attempted to elucidate the effect of creased soft substrate on stem cell behavior [37]. The results showed that neural stem cells can sense the surface creases and formed neurite branches along the creases, while the cells on the smooth pAAM substrate uniformly attached and differentiated.

Other interesting instability behaviors have been found when arranging layers of pAAm/SA hydrogels with dissimilar swelling and mechanical properties.

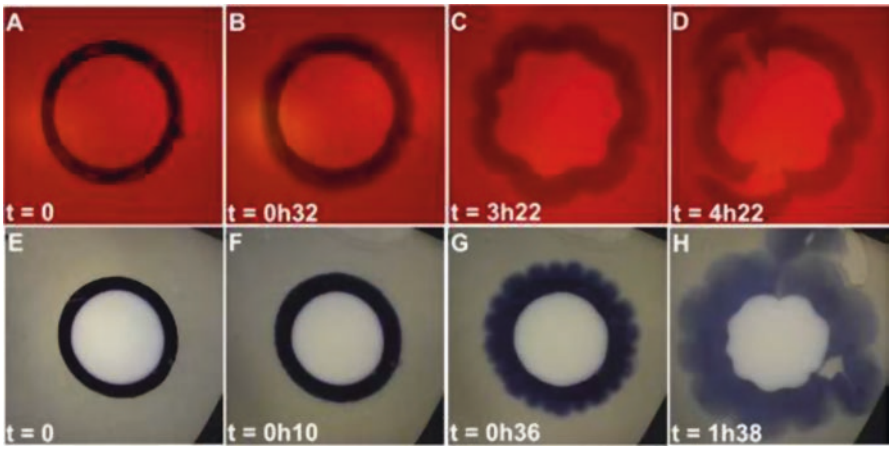

Fig. 9.7 Evolution of two systems composed of two parts: a neutral hydrogel in the center (diameter A, elastic modulus μ_{I}) and a swelling hydrogel layer (thickness H, elastic modulus μ_{II}). Both systems have a similar initial ratio of H/A~0.26–0.27 but with different ratio of elastic modulus. (**A**–**D**) $\mu_{\mathrm{I}} \lesssim \mu_{\mathrm{II}}$, a buckling pattern appears in the ring and at the inner interface; (**E**–**H**) $\mu_{\mathrm{I}} \gtrsim \mu_{\mathrm{II}}$, only the ring forms sharp creases. (Reproduced with permission from Ref. [5])

Folding was demonstrated by chemically bonding two layers of pAAM/SA gels with a stiff and swelling layer on top of a soft and non-swelling layer [29]. In the study, a numerical model for predicting equilibrium folding configurations was proposed, in which the surface instability was represented by a set of self-avoiding rods on a Winkler foundation. The calculated results showed that the amplitude and wavelength of the surface oscillations exhibited a linear dependence of the film thickness and the numerical equilibrium configurations show closer proximity with experimental results than the classical buckling analysis. Other arrangements have been reported including strip geometry, in which two gels were connected by their edges [38]; and the corona geometry, in which a thin corona of the soft gel was attached to a disk of stiff gel [5]. For example, Dervaux et al. designed an artificial tumor model using two layers of pAAM/SA arranged in a corona geometry (Fig. 9.7) [5]. Various patterns were observed in the swelling layer or at the free boundary by changing the ratio of the modulus and thickness between the corona and center region. This study shed light on the correlation between cell geometry, mechanical properties, and their morphological evolution and metastasis potential.

Pattern formation and evolution have also been investigated during the shrinking process. In contrast to the swelling pattern, the shrinking patterns are metastable, have short lifetimes, and are less studied [39]. Li et al. investigated the shrinking patterns of pAAM/SA in acetone/water mixture [39]. When the concentration of acetone (a bad solvent for pAAm) increased, patterns including hexagons, grains, and bubbles were observed due to the formation of a dense surface during the shrinking process.

9.3.1.2 Poly(Hydroxyethyl Methacrylate) (polyHEMA)

PolyHEMA hydrogels have found extensive uses in biomedical field, such as soft contact lenses [40], bone implants [41], and drug delivery system [42–43] because they are highly biocompatible, transparent, and resistant to heat and acid/alkaline hydrolysis [44]. The ability to generate patterned structures in this widely used hydrogel would enable remarkable progress in their applications. The procedure to develop wrinkled patterns in polyHEMA films with a modulus gradient along the film thickness was first reported by Guvendiren et al. using a two-step UV curing process [18]. The procedure involved the irradiation with UV light to a solution composed of HEMA monomers and photoinitiators (Darocur 1173) that was then followed by the second round of UV exposure in the presence of air after adding additional photoinitiator and cross-linker (ethylene glycol dimethacrylate, EGDMA). Due to oxygen diffusion during the UV cross-linking process, a modulus gradient along depth was created. Upon swelling, various instability patterns including random worms, lamellae, peanuts, and long-range ordered hexagonal patterns were observed by varying concentrations of cross-linker, and the wrinkle wavelengths were found to be dependent only on the initial film thickness. In addition, they found that as the cross-linker concentration was increased, the modulus gradient increased and hence the critical osmotic pressure to induce wrinkles. Therefore, the critical osmotic pressure and the resulted patterns can be easily tuned by the modulus gradient. A second publication by the same research group examined the kinetics of the wrinkle evolution at the early stage and at the equilibration states in water (Fig. 9.8) [16]. They found that the characteristic wavelength of the patterns increased with the square root of time at early stages and reached an equilibrium plateau. The swelling ratio α_c for the onset of wrinkling was reported as ~1.12, which was independent of the investigated EGDMA concentration but decreased with increasing film thickness. In contrast, the swelling ratio at the equilibrium state α_e decreased significantly, from 2.55 to 1.2, with increasing cross-linker concentration (from 0 to 3 wt.%). Another study from the same research group examined the transition of wrinkling to creasing instability by manipulating solvent quality [17]. In a good solvent, such as alcohol and alcohol/water mixture, the network was highly swollen. The resulting large volume change induced surface instability from wrinkling to creasing (Fig. 9.8). By changing the ratio of ethanol and water, reversible switching between wrinkling and creasing was obtained. In addition, they found that the swelling ratio for the onset of creasing depended on cross-linker concentration: $\alpha_c \approx 2$ and 1.3 for gels with 1 and 3 wt% EGDMA, respectively.

The polyHEMA-wrinkled patterns have been used for experiments involving cell culture. Wrinkling of lamellar and hexagonal patterns was used by Guvendiren et al. for the study of stem cell response to surface topography [45]. By culturing human mesenchymal stem cell (hMSCs) on hydrogels with uniform mechanics using a replica molding technique, they showed that hMSCs exhibited high aspect ratios and differentiated into an osteogenic lineage on lamellar wrinkles, while hMSCs cultured on hexagonal patterns led to rounded shape with low spreading and differentiated toward an adipogenic phenotype (Fig. 9.9). Moreover, Zhao and coworkers showed that the patterned nonadhesive polyHEMA hydrogel films

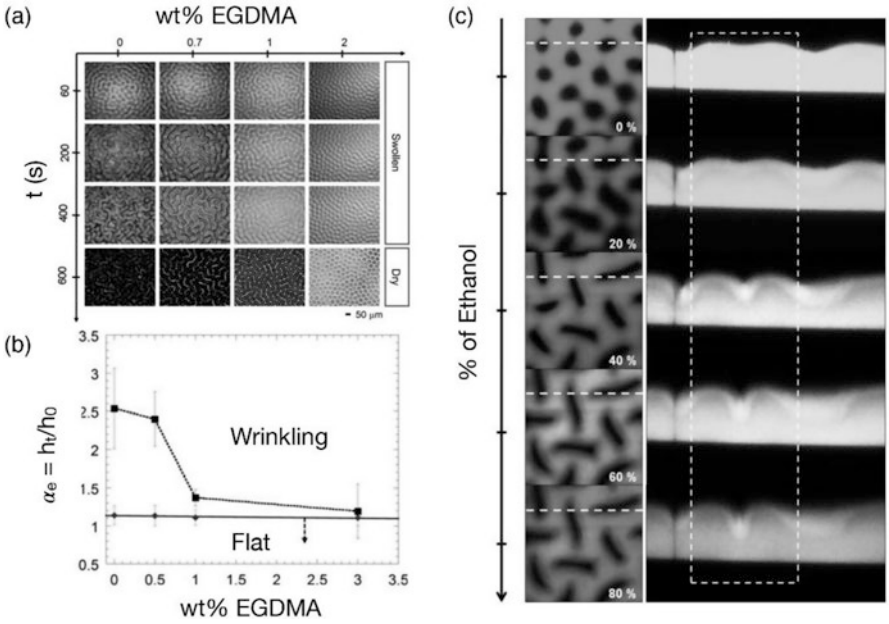

Fig. 9.8 (**a**) Optical microscopy images showing the evolution of swelling patterns of polyHEMA hydrogels as a function of the degree of cross-linking. (**b**) The dependence of equilibrium expansion ratio (α_e) on cross-linkers concentration. The solid line shows the critical expansion ratio (α_c) for the onset of wrinkling. (**c**) Confocal microscopy images of the cross sections of polyHEMA films (3 wt.% EGDMA) showing the dynamic evolution from wrinkling to creasing instability when ethanol was gradually added to the system. (Reproduced with permission from Ref. [16] (**a** and **b**) and [17] (**c**))

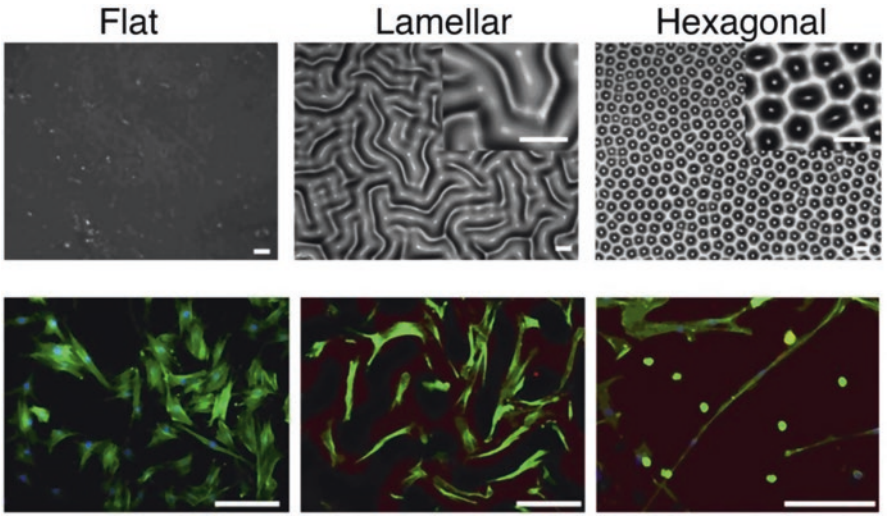

Fig. 9.9 (Top panel) polyHEMA gels containing 1 wt.% EGDMA with different surface patterns. Scale bars are 50 mm (bottom panel). Fluorescent microscopy images of hMSCs seeded on the corresponding hydrogel patterns. Scale bars are 100 mm. (Reproduced with permission from Ref. [45])

were allowed for the high-throughput generation of multicellular spheroids [46]. Thousands of monodisperse spheroids could be easily produced within a single polyHEMA-coated well.

Recently, Gu et al. developed a simpler one-step UV curing method to fabricate the wrinkling patterns on the polyHEMA system [47]. The one-step method involved introducing linear polyHEMA directly into the solutions containing HEMA monomers, cross-linkers EGDMA, and photoinitiators Darocur 1173 and exposing the solution to UV light only one time. The addition of linear polyHEMA allowed for a 3D physical network to form in the solution which stabilized the skin layer and prevented the surface of the film from becoming corrugated after the UV curing process. With the non-corrugated, smooth PHEMA films, the group was able to generate various wrinkling patterns, including the types presented by Guvendiren et al., by changing both the linear polyHEMA and cross-linker concentrations. Li et al. demonstrated another method of creating a gradient of cross-linking density within the polymer films via reactive silane infusion into hydrogel films. During the infusion process, silane reacted with the hydroxyl groups of the polyHEMA polymer and condensed with itself, resulting in a gradient cross-linked top layer and a uniform uncross-linked bottom layer. Subsequent solvent swelling triggered the formation of nano- to micro-scale patterns [15].

9.3.1.3 Poly(Vinyl Alcohol) (PVA)

Inspired by the wrinkling behavior observed when human skin is exposed to water for prolonged periods of time, Zeng et al. created various moisture-sensitive film-substrate bilayer devices, composed of a UV-cross-linked poly(vinyl alcohol) PVA film attached to a soft polydimethylsiloxane (PDMS) substrate, to study and control the reversibility and stability of wrinkles [24]. By adjusting the thickness of the PVA film, PVA cross-linking gradient, PVA/PDMS thickness ratio, and PDMS modulus, three distinct types of moisture-induced wrinkling dynamics were obtained: (A) completely reversible wrinkles, (B) irreversible wrinkles, and (C) completely irreversible wrinkles. The film-substrate bilayer device capable of exhibiting completely reversible wrinkling dynamics used a thin and stiff PVA film that was uniformly cross-linked and a thick and soft PDMS. After exposing to a cool mist, wrinkles formed on the PVA film disappeared after drying and reappeared after moisturizing again. The irreversible wrinkling system used the same film and substrate properties used in system A but instead used an uncross-linked PVA film. Wrinkles were observed after the initial exposure to moisture but disappeared after dying and never returned after further exposure to moisture. As described by Zeng et al., the uncross-linked PVA film was able to induce wrinkles, but due to the film not being cross-linked, during the initial exposure to moisture, the modulus continued to decrease until the wrinkles disappeared. Additionally, the wrinkles could not form after further exposure to moisture due to the reduced swelling strain of the PVA and its inability to create the necessary critical compressive stress to induce wrinkles. Finally, the completely irreversible wrinkling system used a thick PVA

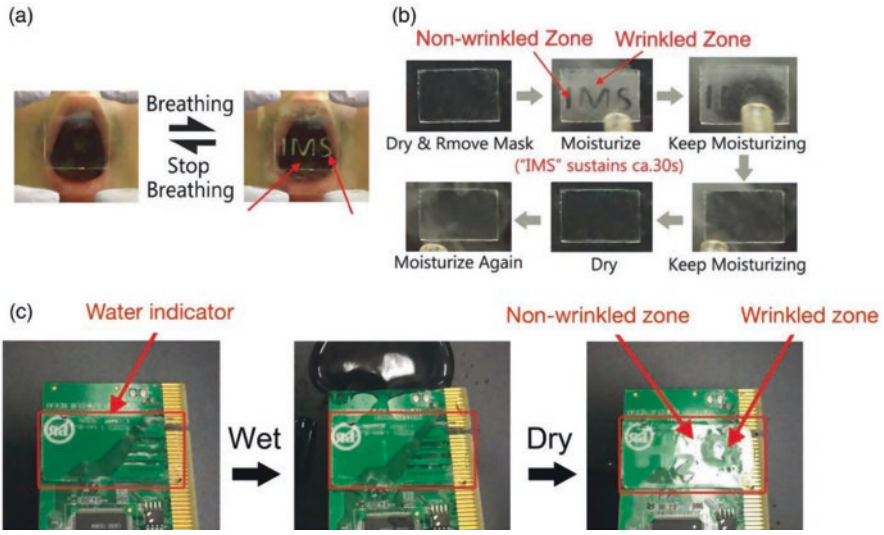

Fig. 9.10 (**a**) The hidden pattern "IMS" was reversibly revealed by breathing on type-A sample. (**b**) The irreversible wrinkling response was demonstrated on type-B PVA films. (**c**) A type-C PVA film which acted as a water indicator was attached to a circuit board. After water exposure and drying the film, the hidden H_2O pattern appeared. (Reproduced with permission from Ref. [24])

film with a cross-linking gradient caused by oxygen inhibition at the surface and a tougher PDMS substrate with a higher elastic modulus. The resulting dynamics consisted of wrinkles that remained even after drying or moisturizing again. The cross-linking gradient allowed the PVA film to exhibit a swelling gradient where the swelling degree gradually decreased along the film depth. When exposed to moisture, the less swollen bottom layers exerted compressive forces to the top layer that were enough to reach the critical stresses required to induce wrinkles. These moisture-responsive systems show many potential applications in optical devices, such as anti-counterfeit tabs, encryption devices, moisture indicators, light diffusers, and antiglare films (Fig. 9.10).

Huraux et al. demonstrated an example of drying-induced morphology on chemically cross-linked PVA gels drying with a free end or with the gels fixed at a constant length [19]. The surface formed wrinkles when drying quickly at low humidity, while the surface remained flat when drying at high humidity. The authors attributed these findings to the crossing of the glass transition temperature of the top hydrogel layer when the drying is fast enough. They proposed the wrinkling was formed following the mechanism that includes three successive steps. First, a concentration gradient was formed due to evaporation from the surface, and the outer skin layer was under stretching. Next, the rapid solvent evaporation caused the skin layer to cross the glass transition temperature, resulting in the formation of a glassy skin layer and the removal of the in-plane tensile tension within the layer. Subsequent solvent evaporation and contraction of the soft bulk layer compressed the glassy skin layer and triggered the formation of wrinkling.

9.3.1.4 Layer-By-Layer Assemblies

In recent years, many studies have focused on ultrathin hydrogel membranes using layer-by-layer (LBL) assembly approach. LBL hydrogel films have been employed for many applications, such as biosensors [48], biocoatings [49], and controlled release [50–51]. The films are fabricated by depositing alternating layers which are bonded through complementary interactions, such as electrostatic attraction, hydrogen bonding, and host-guest interactions [52]. The swelling properties, and thus the resulted surface patterns, can be adjusted by ion type, ionic strength, charge density, film thickness, and deposition method [53]. Swelling-induced surface instability has been observed for hydrogen-bonded LBL multilayer films based on poly(vinyl pyrrolidone) (PVP) and poly(acrylic acid) (PAA) in ethanol/water mixtures (Fig. 9.11) [33]. By changing the composition and pH of the solvent, wrinkles of small and shallow holes were developed via a nucleation-growth process. Unlike most other hydrogels, where critical swelling ratio α_c is insensitive to film thickness [11–12], the critical swelling ratio increased as film thickness increased. It is interesting that in this system, the patterns formed on the constrained hydrogel films disappeared at equilibrium swelling. Normally the restoration of a flat surface when fully swollen is observed only for unconstrained hydrogels. This can be explained by the fact that the thickness of the swollen layer increases with the advancement of swelling, leading to the disappearance of swelling mismatch and thus the relief of compressive stress. The unusual phenomenon found in the constrained PVP/PAA hydrogel films was caused by a different way, in which the rearrangement of hydrogen bonding interactions was recovered between the PVP and PAA chains, leading to the relief of compressive stress. Another example that takes advantage of hydrogen bonding LBL

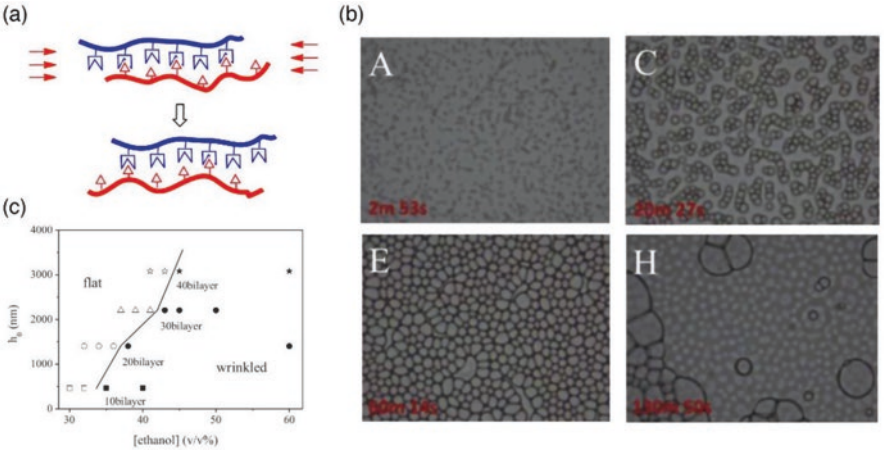

Fig. 9.11 (**a**) Schematic diagram showing the relief of the compressive stress through the rearrangement of the dynamic network of PVP/PAA layers. (**b**) Time evolution of instability morphology of a PVP/PAA 20 bilayer films soaking in 40% ethanol/water mixture. (**c**) Phase diagram showing the transition between the flat and wrinkled surface with different film thickness and ethanol-water ratio. (Reproduced with permission from Ref. [33])

assembly to produce different wrinkling patterns is reported by Hou et al. [53]. Hou and coworkers fabricated (PAA/PEG)*n* on the PDMS substrate, followed by covalently cross-linking with heat. During heating, the water molecules which act as plasticizers were removed, leading to a sharp increase of Young's modulus of (PAA/PEG) *n* films. Wrinkles were formed upon cooling due to thermal expansion mismatch between the rigid cross-linked (PAA/PEG)*n* and the soft PDMS substrate. A sequential and reversible evolution of surface patterns was observed during swelling and deswelling (drying at different elevated temperatures). When immersed into a pH 2.5 aqueous solution, the thermal-induced primary labyrinth wrinkles first disappeared, and then highly ordered hexagonal dimple array appeared. With longer swelling duration, segmented labyrinth patterns were formed. Different surface wrinkling patterns can be reversibly generated by drying, and the resulted deswelled patterns can be finely tuned depending on the swelling-induced patterns and the drying temperatures.

9.3.1.5 Poly(Ethylene Glycol)-Based

Taking advantage of swelling-induced wrinkling, Chan et al. developed a Responsive Surface-wrinkled Adhesive (RSA) using photopolymerized polyethylene glycol methyl acrylate hydrogels uniformly cross-linked with polyethylene glycol dimethacrylate (Fig. 9.12) [54]. The hydrogels were formed on a hemispherical-shaped

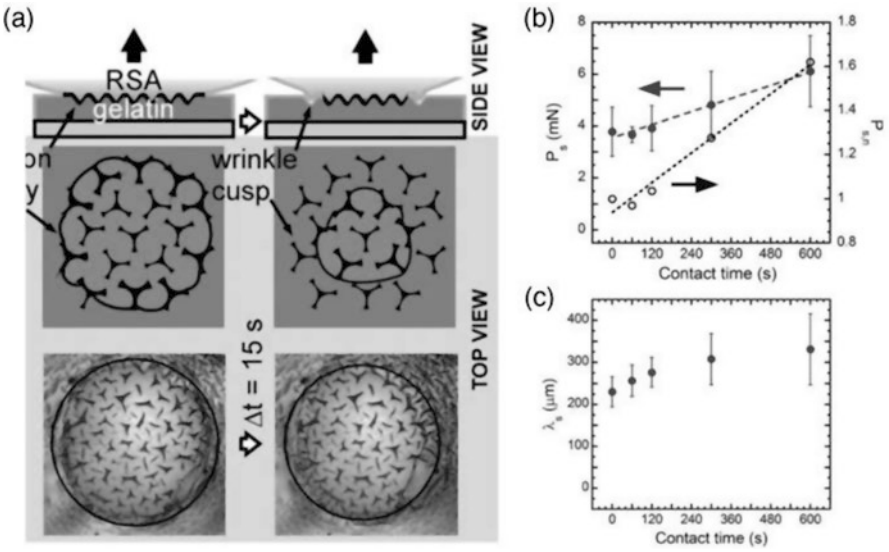

Fig. 9.12 (**a**) Separation process of the RSA-gelatin surface. (**b**) Maximum separation force (P_s) and the normalized separation force ($P_{s,n}$) as a function of contact time for the RSA-gelatin surface. (**c**) Changes in wavelength (λ_s) of wrinkles at P_s versus contact time. (Reproduced with permission from Ref. [54])

cross-linked PDMS mold and brought into contact with a gelatin hydrogel for different periods of time. Enhanced adhesion was observed as the contact time with the gelatin layer was increased. It is commonly known that the increase in adhesion with contact time for dry pressure-sensitive adhesives is due to interdiffusion of polymer chains at the interface, which is highly dependent on chain relaxation time [55]. However, this explanation did not satisfy their observation since the relaxation times of both the RSA and gelatin chains (~1 s for RSA and ~0.01 s for gelatin) are much shorter than the investigated contact times (0, 60, 120, 300, and 600 s). Instead, the authors attributed the enhancement in adhesion to the disruption of crack propagation by locally pinning the crack front by the wrinkled topography. By controlling the time-dependent amplitude and wavelength of wrinkles, the interfacial adhesion can be controlled. This study provided an alternative adhesion mechanism, making it an excellent method for the future development of biomedical adhesives for soft tissues.

9.3.2 Temperature-Induced

9.3.2.1 Poly(*N*-Isopropylacrylamide)(polyNIPAM)-Based

Poly(*N*-isopropylacrylamide) (polyNIPAM) is the most extensively studied thermoresponsive hydrogels for biomedical applications since its low critical solution temperature (LCST) in water is very close to body temperature [56]. In addition, these hydrogels exhibit fast swelling and deswelling in response to temperature change, which make them an ideal platform to study thermal-induced surface instability. The LCST of polyNIPAM in water is around 32 °C, below which, the polymers swell and above which, the polymers shrink. Copolymerization of polyNIPAM with a charged monomer, such as sodium acrylate (SA), is commonly used to increase polymer-water interactions and shift the LCST to a higher temperature, which allows for bringing the transition temperature closer to physiologically relevant temperatures. Earlier findings of constrained gels can be traced back to Li et al. [57], demonstrating the dependence of temperature, time, external constraint, and thermal path, on the shrinking patterns of polyNIPAM-SA gels. The mechanism of the formation and evolution of patterns in shrinking gels showed marked differences than in swelling gels. When gel shrinks, a dense skin layer is formed shielding a swollen gel core. The inhomogeneity in osmotic pressure and polymer concentration in the exterior and interior of the gel drives the formation of patterns. The results showed that the patterns evolved from hexagonal and grain to bubble patterns at temperatures below, near, and above the LCST (Fig. 9.13). Unlike swelling patterns, shrinking patterns are in general metastable or unstable and hard to preserve. The hexagonal, grain, and bubble patterns persisted only for weeks, around 5 h, and about 2 days, respectively. They further employed two different thermal paths: In the first approach (A), gels were abruptly heated from room temperature to

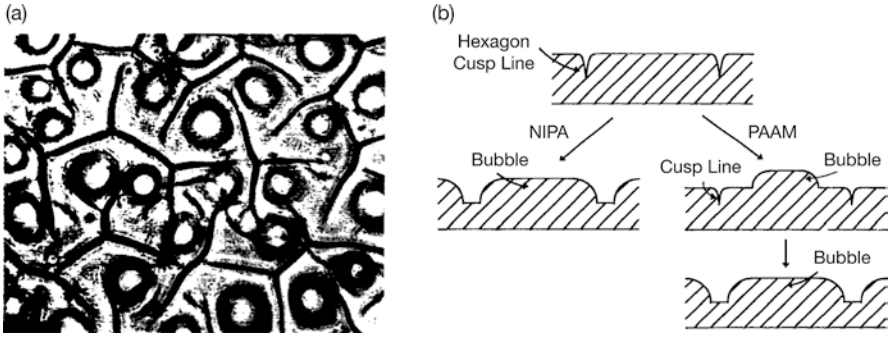

Fig. 9.13 (**a**) The appearance of bubble patterns during thermal shrinkage in the polyNIPAM-SA gels. (**b**) Schematic diagram comparing the formation of bubble patterns in polyNIPAM and pAAM hydrogels. (Reproduced with permission from Ref. [57])

different temperatures (above T_c) and equilibrated for 24 h; In the second approach (B), gels were heated in a stepwise manner at 1 °C per 24 h from room temperature to higher temperatures. Comparing patterns formed under these two routes revealed that the wavelength in A is smaller than that in B, no grain patterns were observed in B, and the wavelength of the hexagonal patterns remained the same in A, while the wavelength increased as the temperature was raised in B. They attributed the difference in the length scale of patterns to differences in shrinking kinetics. The authors also compared the results to the shrinking patterns formed in constrained pAAM gels in acetone/water mixtures [39].

To direct swell-induced crease locations, Kim et al. attached polyNIPAM-SA hydrogels on the substrates with predetermined topographic features [58]. The patterns on the underlying substrates translated into the crease patterns in the hydrogels. At room temperature, the gel swelled and formed self-contact creases, hiding certain areas within the folds. At ~37 °C, the gel deswelled and surface unfolded, exposing the hidden areas and allowing for deposition of biochemically functionalized polyelectrolytes (e.g., poly(L-lysine), peptides, enzymes, and biomolecular ligands) (Fig. 9.14). The hydrogels able to form patterns at desired locations and reversibly hide and display chemical functionality in response to temperature changes show great potential for applications in dynamic cell culture systems. The same research group further investigated the effect of quench depth on the creasing behavior [12]. For shallow quench depth beyond critical strain for the onset of creasing, a crease formed through nucleation and growth, where heterogeneous defects served as nucleation sites. The presence of defects also restricted creases from rearranging and caused strong cycle-to-cycle memory for the crease locations. Precise measurements of critical strain for the onset of creasing ε_M for different film thickness were achieved through measurement of isothermal crease growth velocities at different quench depths. Results showed that as film thickness was reduced, the ε_M slightly increased since the energy barrier caused by gel/water interfacial tension was more pronounced. The transition from wrinkles to folds has been

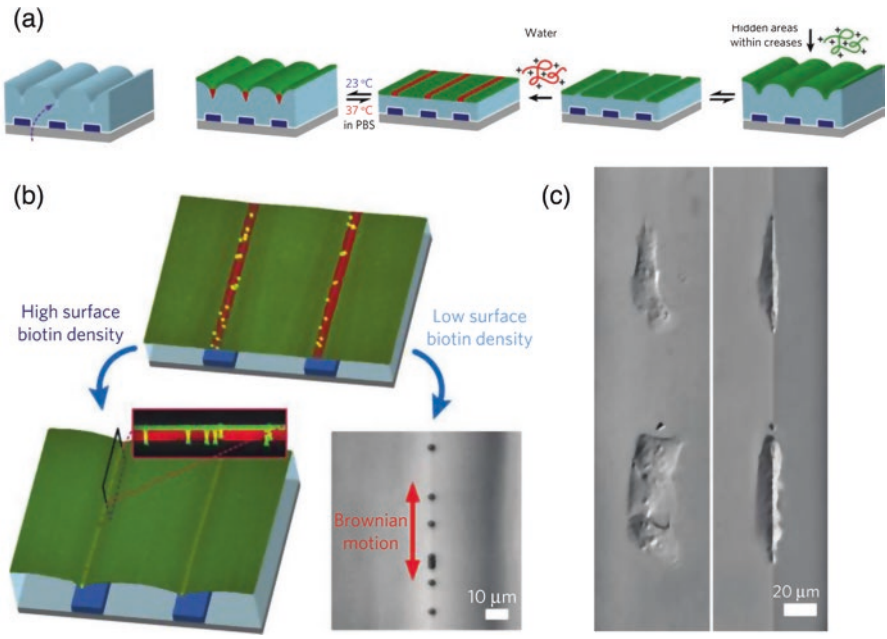

Fig. 9.14 (**a**) Fabrication process of polyNIPAM scaffolds with dynamic display of patterns. (**b**) Streptavidin-coated beads selectively adhered to the biotin-functionalized region (top) at 37 °C. Depending on the biotin density, the beads are either encapsulated within creased (bottom left) or detached from the surface (bottom right) when the scaffold was cooled to 23 °C. (**c**) Optical microscopic images showing the epithelial cells selectively adhered to RGD-functionalized regions at 37 °C (left) and encapsulated within creases at 23 °C (right). (Reproduced with permission from Ref. [58])

reported on bilayer hydrogels composed of a thin crust of silica networks copolymerized with polyNIPAM and a soft bottom layer of polyNIPAM [14]. Reversible wrinkles appeared on cooling, and folding occurred at much lower temperatures. The bilayer hydrogels also showed the peristaltic motion of wrinkles. By controlling the shape of the hybrid silica layer (triangular shape) as well as the cooling rate and temperature, the speed and direction of the peristaltic motion can be modulated, which shows great potential as soft actuators.

9.3.3 Other Types of Stimuli

Other methods which have been reported recently include electric field- and light-induced instability. The use of light and electric field as an external stimulus has the advantages of being easy to employ and generating surface instabilities with

rapid stimuli responses. Xu and Hayward electrically actuated the formation of creases and craters in anionic polyNIPAM hydrogels using low voltages (2–4 V) [25]. The anionic polyNIPAM hydrogel was first deposited on micro-patterned gold electrodes and then swelled in the phosphate-buffered saline (PBS) solution at selective temperatures, to yield a swelling ratio slightly below the onset of creasing. The subsequent application of voltage to underlying electrodes generated creases above the anodes, but not on the cathodes. Observations showed that the electrically driven creases were deeper (crease depth reaches ~70% of the swelled gel thickness) and occurred substantially faster (within a few seconds) compared with the thermally induced patterns. However, the underlying mechanism for the rapid formation of deep electrically driven instability remains unclear, and thus further investigation is required. The same research group reported light-responsive creases based on hybrid gels of anionic polyNIPAM and iron oxide nanoparticles [59]. The authors followed the same approach used in the previous study [58] to create reversible hide and display stripe patterns first. Due to the incorporation of light-absorbance nanoparticles and their strong light-to-heat conversion properties, the heat was generated in hydrogels upon blue light exposure for 3 min. Gels were then deswelled, causing the surface to unfold and expose the hidden areas. After removal of the blue light, creases were reformed over approximately 3 min. The hybrid hydrogel system offers a novel approach to creating a reversible transition between flat states and crease patterns in selected regions by simply exposing light to the interested area.

9.4 Conclusion and Outlook

In summary, many interesting instability patterns and potential applications in hydrogel systems are discussed in this chapter, which are summarized in Table 9.1. A variety of patterns with a different shape, wavelength, and amplitude can be easily generated by manipulating the layer properties (uniform, bilayer, and gradient) and different external stimuli (solvent, thermal, electric field, or light). In particular, recent research has focused on the utilization of hydrogel instability patterns for applications in tissue engineering due to their unique characteristics similar to biological soft tissues. In spite of the extensive work that has been reported, however, many challenges still exist which need further investigation. Expected future studies include large-scale fabrication with precise control of surface patterns; hydrogel exhibiting faster response kinetics (especially for thick films); preparation of patterns at nanometer-scale size; development of “smart” hydrogels with switchable instability patterns; and last but not least, creating surface instability patterns in three-dimensional systems, which could potentially expand their applications.

Table 9.1 Types of hydrogel, surface instability patterns, and potential applications reported in different hydrogel configurations

Layer structure	Top layer	Substrate	Patterns	Stimuli	Applications
Uniform	pAAM [5, 9–12, 15, 37, 39], polyNIPAM [25], [57–59], PVP/PAA LBL films [33], PAA/PEG LBL films [53], PEG-based [54]	Non-swelling PAAM [5], glass slide [10–12, 37, 54, 58–59], petri dish [9], cross-linked PDMS [53–54], silicon wafers [25, 33]	Creases [5, 9–12, 25, 37, 58–59], wrinkles [33, 53–54]	Solvent (swell-induced) [5, 9–12, 33, 37, 53–54], solvent (shrink-induced) [39], thermal (swell-induced) [25, 58–59], thermal (shrink-induced) [57], light [59], electrical field [25]	Artificial tumor models [5], biomedical adhesives [54], dynamic substrates for cellular biology [37, 58], voltage/ light-switchable active surfaces [25, 59]
Layered	pAAM [29], hybrid silica/ polyNIPAM gel [14], stiff PVA [24]	Soft/non-swelling pAAM [29], polyNIPAM [14], PDMS [24], glass slide [58],	Wrinkles [14, 24], folds [14, 29]	Solvent(swell-induced) [24, 29], thermal [14]	Soft actuators [14], optical devices triggered by moisture [24]
Gradient	polyHEMA [15–18, 45–47, 60], PVA [24], dried PVA [19],	Silicon wafers [15, 60], glass slides [17–18, 45–47, 61], PDMS [24], soft PVA [19]	Wrinkles [15, 16, 18, 19, 24, 45–47, 60], creases [17]	Solvent(swell-induced) [15–18, 24, 45–47, 60], solvent(shrink-induced) [19]	Cell culture substrates [45], optical devices triggered by moisture [24], high-throughput generation of cellular spheroids [46]

References

1. A.E. Shyer, T. Tallinen, N.L. Nerurkar, Z. Wei, E.S. Gil, D.L. Kaplan, C.J. Tabin, L. Mahadevan, Villification: How the gut gets its villi. Science **342**(6155), 212 (2013)
2. G. Limbert, E. Kuhl, On skin microrelief and the emergence of expression micro-wrinkles. Soft Matter **14**(8), 1292–1300 (2018). https://doi.org/10.1039/C7SM01969F
3. T. Tallinen, J.Y. Chung, J.S. Biggins, L. Mahadevan, Gyrification from constrained cortical expansion. Proc. Natl. Acad. Sci. **111**(35), 12667 (2014)
4. P. Ciarletta, Buckling instability in growing tumor spheroids. Phys. Rev. Lett. **110**(15), 158102 (2013)
5. J. Dervaux, Y. Couder, M.-A. Guedeau-Boudeville, M. Ben Amar, Shape transition in artificial tumors: From smooth buckles to singular creases. Phys. Rev. Lett. **107**(1), 018103 (2011)
6. J. Rodríguez-Hernández, Wrinkled interfaces: Taking advantage of surface instabilities to pattern polymer surfaces. Prog. Polym. Sci. **42**, 1–41 (2015). https://doi.org/10.1016/j.progpolymsci.2014.07.008
7. S.E. Sheppard, F.A. Elliott, The reticulation of Gelatine. J. Ind. Eng. Chem. **10**(9), 727–732 (1918). https://doi.org/10.1021/ie50105a018

8. P. Thirkell, S. Hoskins, *Continuous Tone Digital Output, Using Archivally Proven Printing Methods and Materials* (Institute of Physics, London, 2003), p. 24
9. T. Tanaka, S.-T. Sun, Y. Hirokawa, S. Katayama, J. Kucera, Y. Hirose, T. Amiya, Mechanical instability of gels at the phase transition. Nature **325**, 796 (1987). https://doi.org/10.1038/325796a0
10. Q. Du, Y. Guan, X.X. Zhu, Y. Zhang, Swelling-induced surface instability patterns guided by pre-introduced structures. Soft Matter **11**(10), 1937–1944 (2015). https://doi.org/10.1039/C4SM02584A
11. V. Trujillo, J. Kim, R.C. Hayward, Creasing instability of surface-attached hydrogels. Soft Matter **4**(3), 564–569 (2008). https://doi.org/10.1039/B713263H
12. J. Yoon, J. Kim, R.C. Hayward, Nucleation, growth, and hysteresis of surface creases on swelled polymer gels. Soft Matter **6**(22), 5807–5816 (2010). https://doi.org/10.1039/C0SM00372G
13. J. Kim, Morphological analysis of crease patterns formed on surface-attached hydrogel with a gradient in thickness. J. Appl. Polym. Sci. **131**(13), 40482 (2014). https://doi.org/10.1002/app.40482
14. Y. Tokudome, H. Kuniwaki, K. Suzuki, D. Carboni, G. Poologasundarampillai, M. Takahashi, Thermoresponsive wrinkles on hydrogels for soft actuators. Adv. Mater. Interfaces **3**(12), 1500802 (2016). https://doi.org/10.1002/admi.201500802
15. Y. Li, J.J. Peterson, S.B. Jhaveri, K.R. Carter, Patterned polymer films via reactive silane infusion-induced wrinkling. Langmuir **29**(14), 4632–4639 (2013). https://doi.org/10.1021/la400155d
16. M. Guvendiren, J.A. Burdick, S. Yang, Kinetic study of swelling-induced surface pattern formation and ordering in hydrogel films with depth-wise crosslinking gradient. Soft Matter **6**(9), 2044–2049 (2010). https://doi.org/10.1039/B927374C
17. M. Guvendiren, J.A. Burdick, S. Yang, Solvent induced transition from wrinkles to creases in thin film gels with depth-wise crosslinking gradients. Soft Matter **6**(22), 5795–5801 (2010)
18. M. Guvendiren, S. Yang, J.A. Burdick, Swelling-induced surface patterns in hydrogels with gradient crosslinking density. Adv. Funct. Mater. **19**(19), 3038–3045 (2009). https://doi.org/10.1002/adfm.200900622
19. K. Huraux, T. Narita, B. Bresson, C. Fretigny, F. Lequeux, Wrinkling of a nanometric glassy skin/crust induced by drying in poly(vinyl alcohol) gels. Soft Matter **8**(31), 8075–8081 (2012). https://doi.org/10.1039/C2SM25480H
20. S.K. Basu, L.E. Scriven, L.F. Francis, A.V. McCormick, Mechanism of wrinkle formation in curing coatings. Prog. Org. Coat. **53**(1), 1–16 (2005). https://doi.org/10.1016/j.porgcoat.2004.08.007
21. S. Yang, K. Khare, P.C. Lin, Harnessing surface wrinkle patterns in soft matter. Adv. Funct. Mater. **20**(16), 2550–2564 (2010). https://doi.org/10.1002/adfm.201000034
22. W.R. Drummond, M.L. Knight, M.L. Brannon, N.A. Peppas, Surface instabilities during swelling of pH-sensitive hydrogels. J. Control. Release **7**(2), 181–183 (1988). https://doi.org/10.1016/0168-3659(88)90010-7
23. A. Ghatak, A.L. Das, Kink instability of a highly deformable elastic cylinder. Phys. Rev. Lett. **99**(7), 076101 (2007)
24. S. Zeng, R. Li, S.G. Freire, V.M.M. Garbellotto, E.Y. Huang, A.T. Smith, C. Hu, W.R.T. Tait, Z. Bian, G. Zheng, D. Zhang, L. Sun, Moisture-responsive wrinkling surfaces with tunable dynamics. Adv. Mater. **29**(24), 1700828 (2017). https://doi.org/10.1002/adma.201700828
25. B. Xu, C. Hayward Ryan, Low-voltage switching of crease patterns on hydrogel surfaces. Adv. Mater. **25**(39), 5555–5559 (2013). https://doi.org/10.1002/adma.201300968
26. M. Kato, Y. Tsuboi, A. Kikuchi, T.-A. Asoh, Hydrogel adhesion with wrinkle formation by spatial control of polymer networks. J. Phys. Chem. B **120**(22), 5042–5046 (2016). https://doi.org/10.1021/acs.jpcb.6b01449
27. B. Li, Y.-P. Cao, X.-Q. Feng, H. Gao, Surface wrinkling of mucosa induced by volumetric growth: Theory, simulation and experiment. J. Mech. Phys. Solids **59**(4), 758–774 (2011). https://doi.org/10.1016/j.jmps.2011.01.010

28. Y. Cao, Y. Jiang, B. Li, X. Feng, Biomechanical modeling of surface wrinkling of soft tissues with growth-dependent mechanical properties. Acta Mech. Solida Sin. **25**(5), 483–492 (2012). https://doi.org/10.1016/S0894-9166(12)60043-3
29. E. Sultan, A. Boudaoud, The buckling of a swollen thin gel layer bound to a compliant substrate. J. Appl. Mech. **75**(5), 051002 (2008). https://doi.org/10.1115/1.2936922
30. E.B. Hohlfeld, *Creasing, Point-Bifurcations, and the Spontaneous Breakdown of Scale-Invariance* (Harvard University, Cambridge, MA, 2008)
31. A.N. Gent, I.S. Cho, Surface instabilities in compressed or bent rubber blocks. Rubber Chem. Technol. **72**(2), 253–262 (1999). https://doi.org/10.5254/1.3538798
32. M.K. Kang, R. Huang, Swell-induced surface instability of confined hydrogel layers on substrates. J. Mech. Phys. Solids **58**(10), 1582–1598 (2010). https://doi.org/10.1016/j.jmps.2010.07.008
33. Q. Han, C. Li, Y. Guan, X.X. Zhu, Y. Zhang, Swelling-induced surface instability of a hydrogen-bonded LBL film and its self-healing. Polymer **55**(9), 2197–2204 (2014). https://doi.org/10.1016/j.polymer.2014.03.015
34. Q. Wang, Zhao, X. A three-dimensional phase diagram of growth-induced surface instabilities. Sci. Rep. **5**, 8887 (2015). https://doi.org/10.1038/srep08887 https://www.nature.com/articles/srep08887#supplementary-information
35. M.A. Biot, Surface instability of rubber in compression. Appl. Sci. Res. Sect. A **12**(2), 168–182 (1963). https://doi.org/10.1007/BF03184638
36. E. Southern, A.G. Thomas, Effect of constraints on the equilibrium swelling of rubber vulcanizates. J. Polym. Sci. Part A Gen. Pap. **3**(2), 641–646 (1965). https://doi.org/10.1002/pol.1965.100030220
37. K. Saha, J. Kim, E. Irwin, J. Yoon, F. Momin, V. Trujillo, D.V. Schaffer, K.E. Healy, R.C. Hayward, Surface creasing instability of soft polyacrylamide cell culture substrates. Biophys. J. **99**(12), L94–L96 (2010). https://doi.org/10.1016/j.bpj.2010.09.045
38. T. Mora, A. Boudaoud, Buckling of swelling gels. Eur. Phys. J. E Soft Matter **20**(2), 119–124 (2006). https://doi.org/10.1140/epje/i2005-10124-5
39. Y. Li, C. Li, Z. Hu, Pattern formation of constrained acrylamide/sodium acrylate copolymer gels in acetone/water mixture. J. Chem. Phys. **100**(6), 4637–4644 (1994). https://doi.org/10.1063/1.466296
40. A. Opdahl, H. Kim Seong, S. Koffas Telly, C. Marmo, A. Somorjai Gabor, Surface mechanical properties of pHEMA contact lenses: Viscoelastic and adhesive property changes on exposure to controlled humidity. J. Biomed. Mater. Res. A **67A**(1), 350–356 (2003). https://doi.org/10.1002/jbm.a.10054
41. G.A. Hutcheon, C. Messiou, R.M. Wyre, M.C. Davies, S. Downes, Water absorption and surface properties of novel poly(ethylmethacrylate) polymer systems for use in bone and cartilage repair. Biomaterials **22**(7), 667–676 (2001). https://doi.org/10.1016/S0142-9612(00)00229-5
42. R.W. Korsmeyer, N.A. Peppas, Solute and penetrant diffusion in swellable polymers. III. Drug release from glassy poly(HEMA-co-NVP) copolymers. J. Control. Release **1**(2), 89–98 (1984). https://doi.org/10.1016/0168-3659(84)90001-4
43. L. Ferreira, M.M. Vidal, M.H. Gil, Evaluation of poly(2-hydroxyethyl methacrylate) gels as drug delivery systems at different pH values. Int. J. Pharm. **194**(2), 169–180 (2000). https://doi.org/10.1016/S0378-5173(99)00375-0
44. J.D. Andrade, Hydrogels for medical and related applications. Am. Chem. Soc. **31**, 380 (1976)
45. M. Guvendiren, J.A. Burdick, The control of stem cell morphology and differentiation by hydrogel surface wrinkles. Biomaterials **31**(25), 6511–6518 (2010). https://doi.org/10.1016/j.biomaterials.2010.05.037
46. Z. Zhao, J. Gu, Y. Zhao, Y. Guan, X.X. Zhu, Y. Zhang, Hydrogel thin film with swelling-induced wrinkling patterns for high-throughput generation of multicellular spheroids. Biomacromolecules **15**(9), 3306–3312 (2014). https://doi.org/10.1021/bm500722g
47. J. Gu, X. Li, H. Ma, Y. Guan, Y. Zhang, One-step synthesis of PHEMA hydrogel films capable of generating highly ordered wrinkling patterns. Polymer **110**, 114–123 (2017). https://doi.org/10.1016/j.polymer.2016.12.076

48. M.M. Barsan, M. David, M. Florescu, L. Ţugulea, C.M.A. Brett, A new self-assembled layer-by-layer glucose biosensor based on chitosan biopolymer entrapped enzyme with nitrogen doped graphene. Bioelectrochemistry **99**, 46–52 (2014). https://doi.org/10.1016/j.bioelechem.2014.06.004
49. M.M. de Villiers, D.P. Otto, S.J. Strydom, Y.M. Lvov, Introduction to nanocoatings produced by layer-by-layer (LbL) self-assembly. Adv. Drug Deliv. Rev. **63**(9), 701–715 (2011). https://doi.org/10.1016/j.addr.2011.05.011
50. P.T. Hammond, Building biomedical materials layer-by-layer. Mater. Today **15**(5), 196–206 (2012). https://doi.org/10.1016/S1369-7021(12)70090-1
51. S. Mehrotra, D. Lynam, R. Maloney, M. Pawelec Kendell, H. Tuszynski Mark, I. Lee, C. Chan, J. Sakamoto, Time controlled protein release from layer-by-layer assembled multilayer functionalized agarose hydrogels. Adv. Funct. Mater. **20**(2), 247–258 (2009). https://doi.org/10.1002/adfm.200901172
52. J. Borges, J.F. Mano, Molecular interactions driving the layer-by-layer assembly of multilayers. Chem. Rev. **114**(18), 8883–8942 (2014). https://doi.org/10.1021/cr400531v
53. J. Hou, Q. Li, X. Han, C. Lu, Swelling/deswelling-induced reversible surface wrinkling on layer-by-layer multilayers. J. Phys. Chem. B **118**(49), 14502–14509 (2014). https://doi.org/10.1021/jp508724n
54. E.P. Chan, J.M. Karp, R.S. Langer, A "Self-Pinning" adhesive based on responsive surface wrinkles. J. Polym. Sci. B Polym. Phys. **49**(1), 40–44 (2011). https://doi.org/10.1002/polb.22165
55. M.M. Feldstein, R.A. Siegel, Molecular and nanoscale factors governing pressure-sensitive adhesion strength of viscoelastic polymers. J. Polym. Sci. B Polym. Phys. **50**(11), 739–772 (2012). https://doi.org/10.1002/polb.23065
56. A. Gandhi, A. Paul, S.O. Sen, K.K. Sen, Studies on thermoresponsive polymers: Phase behaviour, drug delivery and biomedical applications. Asian J Pharm Sci **10**(2), 99–107 (2015). https://doi.org/10.1016/j.ajps.2014.08.010
57. C. Li, Z. Hu, Y. Li, Temperature and time dependencies of surface patterns in constrained ionic N-isopropylacrylamide gels. J. Chem. Phys. **100**(6), 4645–4652 (1994). https://doi.org/10.1063/1.466247
58. J. Kim, J. Yoon, R.C. Hayward, Dynamic display of biomolecular patterns through an elastic creasing instability of stimuli-responsive hydrogels. Nat. Mater. **9**, 159 (2009). https://doi.org/10.1038/nmat2606 https://www.nature.com/articles/nmat2606#supplementary-information
59. J. Yoon, P. Bian, J. Kim, J. McCarthy Thomas, C. Hayward Ryan, Local switching of chemical patterns through light-triggered unfolding of creased hydrogel surfaces. Angew. Chem. **124**(29), 7258–7261 (2012). https://doi.org/10.1002/ange.201202692
60. C.M. González-Henríquez, D.H. Sagredo-Oyarce, M.A. Sarabia-Vallejos, J. Rodríguez-Hernández, Fabrication of micro and sub-micrometer wrinkled hydrogel surfaces through thermal and photocrosslinking processes. Polymer **101**, 24–33 (2016). https://doi.org/10.1016/j.polymer.2016.08.051
61. C. Robert, E. Kamal, W. Honglu, S. Wei, Biofabrication of a three-dimensional liver microorgan as an in vitro drug metabolism model. Biofabrication **2**(4), 045004 (2010)